Acoustic Simulation of an Induction Machine with Squirrel-Cage Rotor

C. Schlensok, D. van Riesen, T. Küest, G. Henneberger

Institute of Electrical Machines (IEM), RWTH Aachen University, Germany
Schinkelstraße 4, D-52056 Aachen, Germany, phone: (+49 241 8 09 76 67), fax: (+49 241 8 09 22 70)
e-mail: Christoph.Schlensok@iem.rwth-aachen.de

I. INTRODUCTION

Due to the customer's satisfaction the acoustics in cars are getting more and more part of research. Nowadays, there are many electromagnetic devices in cars, which have replaced mechanical systems. One example for this trend is an electrical machine replacing the hydraulic power-steering drive. In this paper an induction machine with squirrel-cage rotor is analyzed regarding the electromagnetically excited audible noise. This motor is employed as power-steering drive. The aim of this work is to predict the noise generated by the device. The machine is simulated using the Finite-Element Method (FEM) for the electromagnetic and the structural-dynamic model and the Boundary-Element Method (BEM) for the noise estimation.

II. FEM/BEM SIMULATION

The computational process of acoustic simulation of the induction machine is divided into three steps:

1. electromagnetic FEM simulation,

2. structural-dynamic FEM computation, and the

3. acoustic BEM calculation.

For all three steps models of the machine geometry have to be built and discretized which take the relevant parts of the machine into account, respectively.

ELECTROMAGNETIC SIMULATION

In the case of induction machines with squirrel-cage rotor the rotor-bar currents are unknown. Therefore, a transient calculation, which takes the rotational movement into account, has to be performed. In order to reduce the computation time the machine is calculated in 2 dimensions at first. The $\vec{A}$-formulation used in the solver *i*MOOSE.tsa2d reads:

$$
\begin{aligned}
&\int_{\Gamma} \left(\nabla \alpha_i \cdot \nu \cdot \nabla A_z(t) + \alpha_i \cdot \sigma \cdot \tfrac{\partial}{\partial t} A_z(t) \right) \mathrm{d}\Gamma \\
&= \int_{\Gamma} \left(\alpha_i \cdot J_{z0}(t) + \nabla \times (\alpha_i \vec{e_z}) \cdot \nu \vec{B}_r \right) \mathrm{d}\Gamma, \quad (1) \\
&\qquad \forall\, i = 1, 2, \ldots, n_n \,.
\end{aligned}
$$

The equation given in Galerkin formulation [1] is solved in the entire model region Γ. The material parameters ν and σ represent the non-linear reluctivity and the linear conductivity. The shape function of an element is defined by α_i. First order triangular shaped elements are used. $J_{z0}(t)$ describes the z-component of the given coil current-density and $\vec{B}_r$ is the remanence of possible permanent magnets which of course do not exist

in induction machines. For linear interpolation of the time-dependent variables the first order time-step algorithm is applied and $A(t)$ can be written as a function of time:

$$
\begin{aligned}
A(t) &= (1 - \Theta)\, A_n + \Theta\, A_{n+1} &(2)\\
\Theta &= \frac{t - t_n}{t_{n+1} - t_n} = \frac{t - t_n}{\Delta t}; \qquad 0 \le \Theta \le 1\,. &(3)
\end{aligned}
$$

Θ is the weighting parameter and set to $\Theta = \frac{2}{3}$ according to the Galerkin scheme [2]. Setting $\Theta = \frac{2}{3}$ results in fastest convergence for the transient simulation.

The induction machine regarded has $N_S = 36$ stator and $N_R = 26$ rotor slots. Due to the number of rotor slots the motor shows a 180° symmetry. Therefore, a half (180°) FEM-model is used. The 2D electromagnetic model consists of 6,882 first order, triangular elements. 4,000 time steps are calculated at rated speed $n_N = 1,200\,\mathrm{rpm}$ and a stator frequency of $f_1 = 48.96\,\mathrm{Hz}$. The resulting torque behavior of the transient calculation is shown in Fig. 1. When the transient phenomenon has died out the time behavior is analyzed. The average torque is $\overline{T}_{2D} = 4.312\,\mathrm{Nm}$.
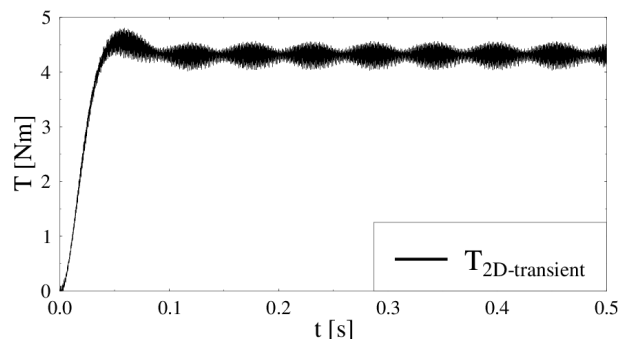

Figure 1: Resulting Torque Obtained from the 2D Model.

With

$$
J_z = -\sigma \frac{A_{z_{n+1}} - A_{z_n}}{\Delta t} \qquad (4)
$$

the rotor-bar current-density J_z is evaluated. A_z is the z-component of the magnetic vector potential $\vec{A}$. The conductivity of the rotor bars is represented by σ. The time step is Δt.

Fig. 2 shows the resulting rotor-bar currents for four bars. The frequency is the slip frequency $f_2 = 8.96\,\mathrm{Hz}$. The maximal current amplitude reached for all bars is $I_{max} = 248.32\,\mathrm{A}$ and the amplitude of the fundamental is $\hat{I}_1 = 220.86\,\mathrm{A}$. The first significant harmonic order is the fifth order of the stator frequency at $f_5 = 244.8\,\mathrm{Hz}$ with $\hat{I}_5 = 23.15\,\mathrm{A}$ which is modulated with twice the slip frequency: $f = 226.88\,\mathrm{Hz}$ and $f = 262.72\,\mathrm{Hz}$.
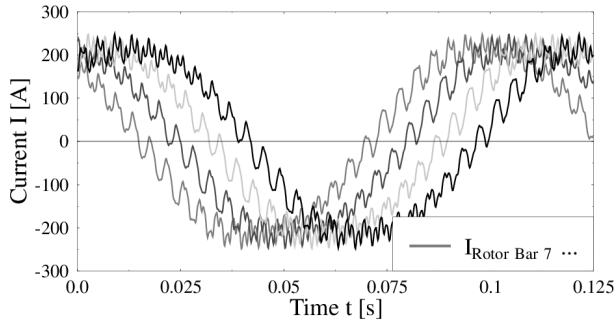
Figure 2: Resulting Rotor-Bar Currents for Four Rotor Bars Obtained from the 2D Model.

The resulting current densities are used by the static, 3-dimensional FEM model, which computes the machine using *i*MOOSE.stat3d. The 3D static electromagnetic solver formulation applying the magnetic vector potential $\vec{A}$ in Galerkin scheme reads [3]:

$$\int_{\Omega} \nabla \times \vec{\alpha_i} \cdot \nu \cdot \nabla \times \vec{A} \, d\Omega$$
$$= \int_{\Omega} \left(\vec{\alpha_i} \cdot \vec{J_0} + \nabla \times \vec{\alpha_i} \cdot \nu \vec{B_r} \right) d\Omega, \qquad (5)$$
$$\forall \, i = 1, 2, \dots, n_n \, .$$

Both solvers from equations (1) and (5) are part of the open-source software *i*MOOSE [4].

The FEM-model consists of 288,782 first order tetrahedral elements. For computation-time saving-reasons the axial length of the model is reduced to a third of the iron length. The skewing angle (front to back angle) is kept the same. Fig. 3 shows the electromagnetic model of the motor.
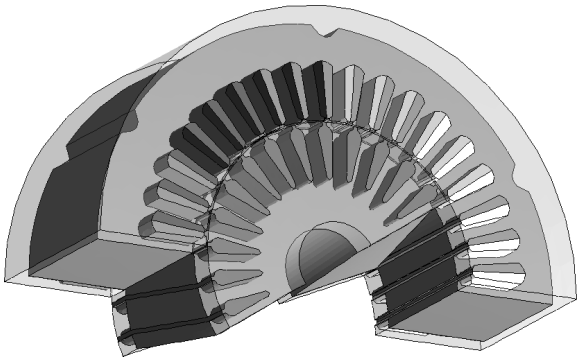

Figure 3: 3D FEM Model for Electromagnetic Simulation.

The stator winding head and the short-circuit ring of the rotor are reduced to extended bars, which are surrounded by air. This allows a more realistic consideration of the front leakage than in case of the 2D model. There, of course no front leakage can be regarded. The figure also shows the two-layer winding of the stator and the complicated modeling of the skewed rotor. To avoid the slicing of rotor bars which would result in very difficult to compute current excitations the rotor is modeled in such a way that it is twisted in the same way the bars are.

The machine is calculated at $N = 120$ rotor positions. The skewing of the rotor is kept the same.

The mechanical angle between each static time step is $\Delta \alpha = 3°$. The machine's skewing angle is $\gamma = 10°$. For each time step the rotor is detached from the stator, rotated, and reattached. The models are generated automatically with the FEM-tool ANSYS [5]. Fig. 4 shows the flux-density distribution for one time step exemplary.
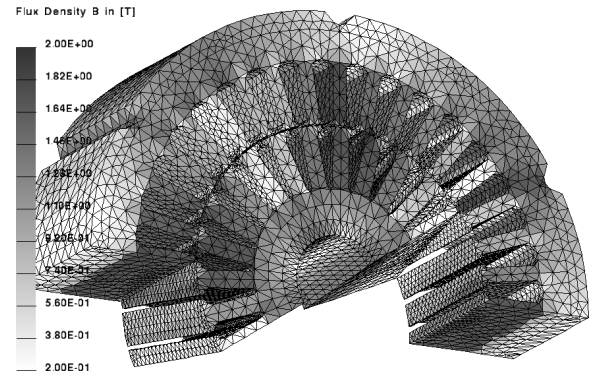

Figure 4: Flux-Density Distribution for the 3D Model.

STRUCTURAL-DYNAMIC SIMULATION

From the flux-density distribution the surface-force density on the stator teeth can be derived using the Maxwell-stress tensor [3][6]. The formulation reads:

$$\vec{\sigma} = \frac{1}{2} \vec{n}_{12} \left[B_n \left(H_{1n} - H_{2n} \right) - \left(w_1' - w_2' \right) \right] . \qquad (6)$$

The index n represents the normal components of $\vec{B}$ and $\vec{H}$. $\vec{n}_{12}$ is the normal vector of the boundary surface from region 2 to 1. w_1' and w_2' are the magnetic co-energy densities of these regions. Lorentz forces and forces stemming from magnetostriction can be neglected since they are much lower than the electromagnetic forces.

Fig. 5 shows the surface-force density distribution for one time step. The skewing of the rotor is reflected
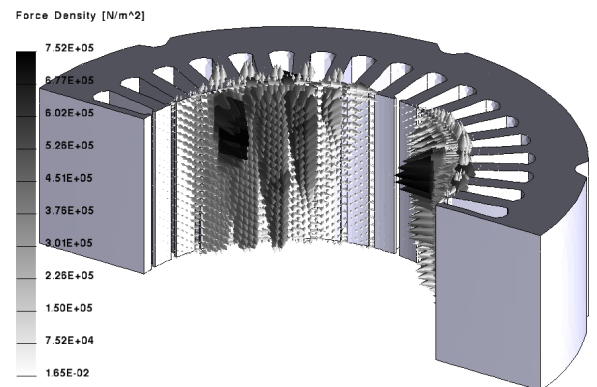

Figure 5: Surface-Force Density Distribution on the Stator Teeth for One Time Step (Only Stator Lamination Shown).

in the force excitation of the stator teeth. Depending on the rotational direction the up-running edge of each tooth is excited highest on the front or on the back side.
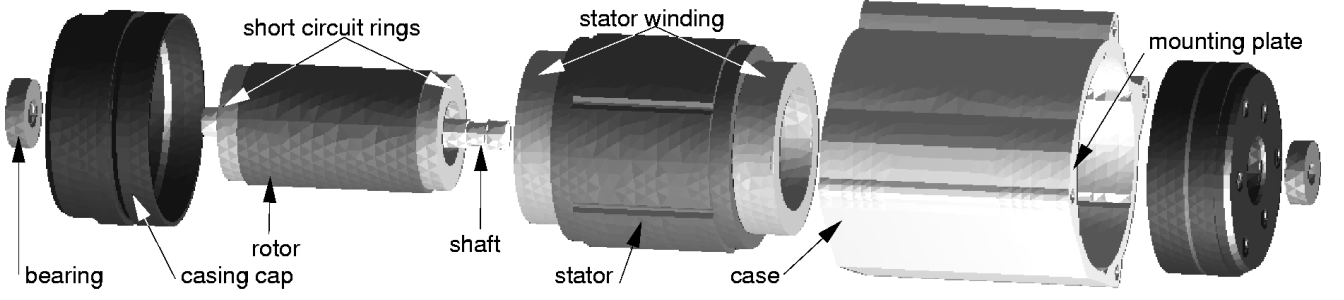
Figure 6: Exploded View of the Structure-Dynamic Model of the Induction Machine with Squirrel-Cage Rotor.

In a next step the force excitation has to be analyzed. For each element of the stator teeth connected to the air gap the values of all time steps are collected and then transformed into the frequency domain using the Fast-Fourier Transformation (FFT) [7]. This is a very time intensive step in the acoustic analysis of an electrical machine, because the data is distributed to each time step but must be assigned to each element. This means, that for each of the 20,602 stator-teeth surface elements which are connected to the air gap, 120 force-density values must be collected and analyzed using the FFT. Finally the FFT values must be resorted to two files per frequency which hold the imaginary and the real part of the surface-force density excitation. The resulting spectrum (absolute values) for one single stator-tooth element is depicted in Fig. 7.
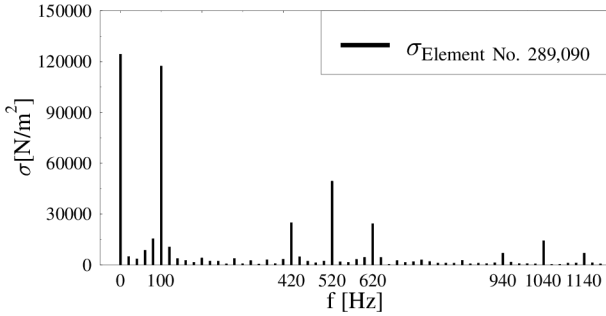

Figure 7: Spectrum of the Surface-Force Density Excitation of One Single Stator-Tooth Surface Element (Absolute-Values).

Due to the time step Δt and the number of time steps N the cut-off frequency is $f_{co} = 1,200\,\text{Hz}$ with $\Delta f = 20\,\text{Hz}$ which is equal to the rotor speed. The harmonic orders detected in the spectrum are the double stator frequency ($97.92\,\text{Hz}$), the first and second rotor slot harmonic ($520\,\text{Hz}$ and $1040\,\text{Hz}$), and their modulations with the double stator frequency [8][9][10]. The harmonic orders with the highest magnitudes are selected for the further study.

The next step is to calculate the deformation of the entire structure of the machine. Therefore, a complete mechanical model of the machine must be generated consisting of the stator and rotor with their windings, the shaft, the case, the bearings, and the casing caps. In order to reduce the number of finite elements the rotor is simplified and modeled as a cylinder. The sta-

tor tooth geometry is reduced to a rectangular shape. The number of first order tetrahedral elements of the mechanical model is 90,065. The solver transforms the first order elements to second order. Fig. 6 shows an exploded view of the entire model.

With the mechanical model the deformation of the structure of the induction machine is computed for the selected frequencies in the following step. Therefore, the surface-force density excitation is transformed from the electromagnetic model to the mechanical model for each of the selected frequencies.

The deformation-solver formulation reads [11]:

$$\boldsymbol{K} \cdot \boldsymbol{D} + \boldsymbol{F} \cdot \dot{\boldsymbol{D}} + \boldsymbol{M} \cdot \ddot{\boldsymbol{D}} = \boldsymbol{R}. \qquad (7)$$

$\boldsymbol{K}$ is the matrix of the stiffness of all elements of the model, $\boldsymbol{M}$ represents the mass, $\boldsymbol{F}$ is the damping, $\boldsymbol{D}$ is the deformation, and $\boldsymbol{R}$ is the exciting force. Due to harmonic analysis (7) is simplified to:

$$(\boldsymbol{K} - \omega^2 \cdot \boldsymbol{M} + j\omega \cdot \boldsymbol{F}) \cdot \boldsymbol{D} = \boldsymbol{R}. \qquad (8)$$

$\omega = 2\pi f$ is the angular frequency. The damping $\boldsymbol{F}$ can be neglected since the mechanical model is built of material with high elastic stress modules. If for instance rubber is used the damping cannot be neglected. Therefore, the solver is not able to regard such elastic materials. Initial tension is not regarded as well. Usually, initial tension mainly arises from temperature effects which are not subject of the investigations.

$\boldsymbol{K}$ is the sum of all element-stiffness matrices $\boldsymbol{k}_i$:

$$\boldsymbol{K} = \sum_{i=1}^{n} \boldsymbol{k}_i = \sum_{i=1}^{n} \int_{\Omega_i} \boldsymbol{B}_i^T \cdot \boldsymbol{H}_i \cdot \boldsymbol{B}_i \, d\Omega_i. \qquad (9)$$

$\boldsymbol{H}_i$ is the elasticity matrix for each element [2]:

$$\boldsymbol{H}_i =$$

$$\frac{E \cdot (1-\nu)}{(1+\nu) \cdot (1-2\nu)} \cdot \begin{pmatrix} 1 & a & a & 0 & 0 & 0 \\ a & 1 & a & 0 & 0 & 0 \\ a & a & 1 & 0 & 0 & 0 \\ 0 & 0 & 0 & b & 0 & 0 \\ 0 & 0 & 0 & 0 & b & 0 \\ 0 & 0 & 0 & 0 & 0 & b \end{pmatrix}, \qquad (10)$$

with

$$a = \frac{\nu}{1-\nu} \quad \text{and} \quad b = \frac{1-2\nu}{2(1-\nu)}. \qquad (11)$$

ν is Poisson's ratio and E the elastic modulus. $\boldsymbol{B}_i$ is the differential matrix for the elements, where $\boldsymbol{B}_i^T$ is

the transposed of it. With $\alpha_1 \ldots \alpha_4$ being the degrees of freedom of the first-order tetrahedral elements $\boldsymbol{B}_i$ reads [11]:

$$\boldsymbol{B}_i = \begin{pmatrix} \frac{\partial \alpha_1}{\partial x} & 0 & 0 & \cdots & \frac{\partial \alpha_4}{\partial x} & 0 & 0 \\ 0 & \frac{\partial \alpha_1}{\partial y} & 0 & \cdots & 0 & \frac{\partial \alpha_4}{\partial y} & 0 \\ 0 & 0 & \frac{\partial \alpha_1}{\partial z} & \cdots & 0 & 0 & \frac{\partial \alpha_4}{\partial z} \\ \frac{\partial \alpha_1}{\partial y} & \frac{\partial \alpha_1}{\partial x} & 0 & \cdots & \frac{\partial \alpha_4}{\partial y} & \frac{\partial \alpha_4}{\partial x} & 0 \\ 0 & \frac{\partial \alpha_1}{\partial z} & \frac{\partial \alpha_1}{\partial y} & \cdots & 0 & \frac{\partial \alpha_4}{\partial z} & \frac{\partial \alpha_4}{\partial y} \\ \frac{\partial \alpha_1}{\partial z} & 0 & \frac{\partial \alpha_1}{\partial x} & \cdots & \frac{\partial \alpha_4}{\partial z} & 0 & \frac{\partial \alpha_4}{\partial x} \end{pmatrix} \quad (12)$$

The matrices $\boldsymbol{M}$, $\boldsymbol{F}$, $\boldsymbol{D}$, and $\boldsymbol{R}$ of equations (7) and (8) are built in an analogue way to $\boldsymbol{K}$ from equation (9). In order to solve the boundary-value problem of the deformations entirely a boundary condition must be regarded. It is necessary to define at least one node of the model which is fixed. This is a Dirichlet condition. Here, the surface nodes of the mounting plate are selected and fixed in the solving process (see Fig. 6).

Fig. 8 shows exemplarily the strongly emphasized real part of the deformation of the stator lamination and the casing for $f = 620\,\mathrm{Hz}$. The emphasizing factor is set to 6,750,000.

(a) Deformation of Stator and Casing.
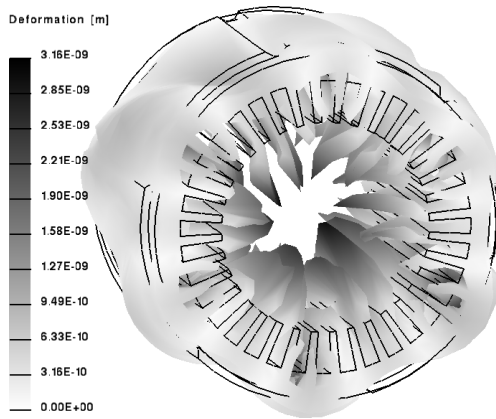
(b) Deformation of Stator.

Figure 8: Real Part of the Deformation for $f = 620\,\mathrm{Hz}$.

Due to the even number of pole pairs $p = 2$ and the even number of rotor slots $N_R = 26$ of the induction machine the mechanical orders of deformation can only be even numbers as well: $r = 0, 2, 4, \ldots$ [12]. Some orders found are depicted in Fig. 9. $r = 2$ is found

for $f = 720\,\mathrm{Hz}$, $r = 4$ for $f = 1040\,\mathrm{Hz}$, and $r = 6$ for $f = 620\,\mathrm{Hz}$. Small mechanical orders have the strongest impact in respect of the deformation amplitude. For this reason numbers greater than $r = 6$ can be neglected in general.

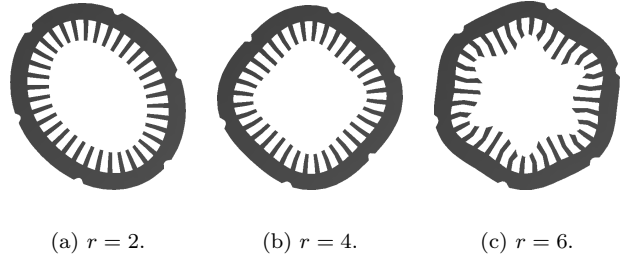(a) $r = 2$.   (b) $r = 4$.   (c) $r = 6$.

Figure 9: Mechanical Orders of the Deformation.

The deformation of the structure of the machine can be used for the acoustic simulation described in the following section. Alternatively the structure-borne sound can be derived from its results. Here, simulation results are compared to acceleration measurements performed by the industrial partner. The reference value is $a_{ref} = 1\,\frac{\mu\mathrm{m}}{\mathrm{s}^2}$ and the level L_S is defined by:

$$L_S = 20 \cdot \log \frac{a}{a_{ref}} \, \mathrm{dB}\,. \quad (13)$$

a is the acceleration of the specific node at the regarded frequency f, which is derived from the displacement u. $\omega = 2\pi f$ is the angular frequency. In respect of the sinusoidal deformation the acceleration vector is defined by:

$$\vec{a} = \begin{pmatrix} a_{tan} \\ a_{rad} \\ a_{axial} \end{pmatrix} = \begin{pmatrix} -\omega^2 \cdot u_{tan} \\ -\omega^2 \cdot u_{rad} \\ -\omega^2 \cdot u_{axial} \end{pmatrix} \text{ with } \quad (14)$$

$$\frac{\partial^2 u(t)}{\partial t^2} = \frac{\partial^2}{\partial t^2} \hat{u} \cdot \cos(\mathrm{j}\omega t - \varphi) = -\omega^2 \cdot u(t)\,. \quad (15)$$

φ is the phase angle and $j^2 = -1$. The displacement is a vector of complex numbers in Cartesian coordinates:

$$\underline{\vec{u}} = \begin{pmatrix} \underline{x} \\ \underline{y} \\ \underline{z} \end{pmatrix} = \begin{pmatrix} \Re\{\underline{x}\} + j\Im\{\underline{x}\} \\ \Re\{\underline{y}\} + j\Im\{\underline{y}\} \\ \Re\{\underline{z}\} + j\Im\{\underline{z}\} \end{pmatrix}\,. \quad (16)$$

In order to provide the displacement vector as local coordinates with tangential, radial, and axial component the following transformation has to be performed:

$$\vec{\underline{u}}_{local} = \begin{pmatrix} \underline{u}_{tan} \\ \underline{u}_{rad} \\ \underline{u}_{axial} \end{pmatrix} = \begin{pmatrix} \underline{\vec{u}} \cdot \vec{e}_{tan} \\ \underline{\vec{u}} \cdot \vec{e}_{rad} \\ \underline{\vec{u}} \cdot \vec{e}_{axial} \end{pmatrix}$$

$$= \begin{pmatrix} \underline{x} \cdot \vec{e}_x \cdot \vec{e}_{tan} + \underline{y} \cdot \vec{e}_y \cdot \vec{e}_{tan} + \underline{z} \cdot \vec{e}_z \cdot \vec{e}_{tan} \\ \underline{x} \cdot \vec{e}_x \cdot \vec{e}_{rad} + \underline{y} \cdot \vec{e}_y \cdot \vec{e}_{rad} + \underline{z} \cdot \vec{e}_z \cdot \vec{e}_{rad} \\ \underline{x} \cdot \vec{e}_x \cdot \vec{e}_{axial} + \underline{y} \cdot \vec{e}_y \cdot \vec{e}_{axial} + \underline{z} \cdot \vec{e}_z \cdot \vec{e}_{axial} \end{pmatrix}\,. \quad (17)$$

The three components of the local coordinate systems are equal to those of a global cylindrical coordinate system with the axial component in direction of the shaft,

the radial is normal onto the rotor cylinder and the tangential in direction of the angle φ [7].

Table 1 shows some results of the structure-borne sound-simulation. The highest amplitudes are reached for the first rotor-slot harmonic at $f_{26} = 26 \cdot f_R = 520\,\mathrm{Hz}$, the first stator-slot harmonic $f_{36} = 36 \cdot f_R = 720\,\mathrm{Hz}$, $f = 940\,\mathrm{Hz}$, and $f = 1040\,\mathrm{Hz}$. The level for the axial component shows the smallest values in all cases. These results suit the acceleration measurements performed by the industrial partner very well.

Table 1: Results of the Structure-Borne Sound-Simulation.

f [Hz]	$L_{S,rad}$ [dB]	$L_{S,tan}$ [Hz]	$L_{S,axial}$ [dB]
100	59.4	58.5	44.0
420	85.2	83.8	68.4
520	82.6	82.1	66.9
620	59.9	64.5	48.5
720	85.4	84.2	68.8
940	88.5	87.5	46.8
1040	82.4	80.5	55.7
1140	67.7	67.0	51.4

ACOUSTIC SIMULATION

The last step of the analysis is the acoustic simulation of the machine. Acoustic noise is a result of the deformation of the surface of a body. Therefore, only the deformation of the surfaces has to be taken into account and the Boundary-Element Method (BEM) is applied for the acoustic computation. The equation to be solved reads:

$$\boldsymbol{H} \cdot \underline{p} = \boldsymbol{G} \cdot \underline{\vec{v}}. \tag{18}$$

$\underline{p}$ is the complex sound pressure which is the result of the acoustic simulation and $\underline{\vec{v}}$ is the complex velocity vector of all nodes of the BEM model.
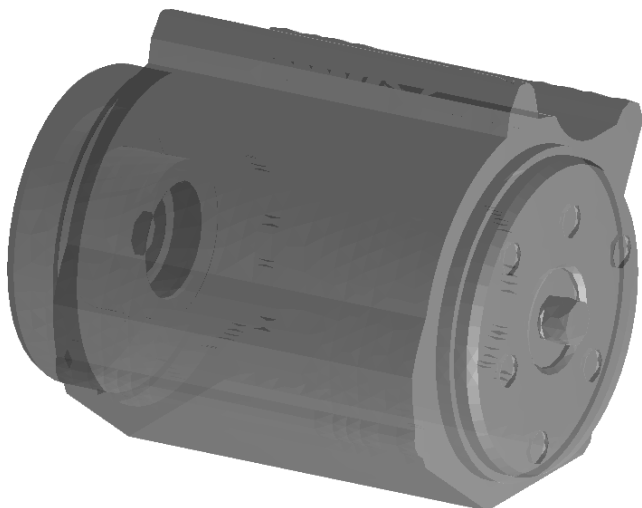

Figure 10: The Acoustic Model of the Machine.

For the acoustic simulation a third model of the machine is generated by extracting the surface mesh of the structural-dynamic model. The resulting model consists of 7,998 triangular shell elements (Fig. 10).

After the acoustic model has been computed the sound pressure is estimated in a post-processing step. An analysis hemisphere is located in a distance of $d = 1\,\mathrm{m}$ around the machine. The induction machine is positioned in the center of the ground plane. The ground plane itself is reverberant. Of course, different analysis surfaces like spheres and planes are possible. On the surface of the hemisphere the sound pressure p from equation (18) is computed. The values of the sound pressure spread over a wide range. For this reason the sound-pressure values are written as a level:

$$L_p = 20 \cdot \log\left(\frac{p}{p_0}\right)\,\mathrm{dB}. \tag{19}$$

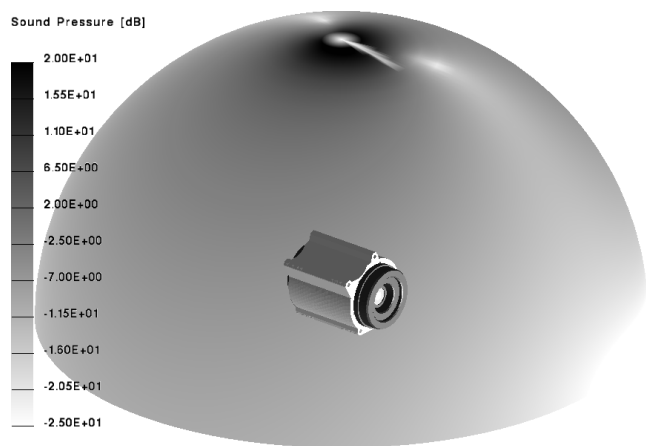$p_0 = 2 \cdot 10^{-5}\,\frac{\mathrm{N}}{\mathrm{m}^2}$ is the auditory threshold at $1,000\,\mathrm{Hz}$.

Figure 11: Sound-Pressure Distribution for $f = 520\,\mathrm{Hz}$.

Fig. 11 depicts exemplarily the sound-pressure distribution for $f = 520\,\mathrm{Hz}$. There are some extinction effects on the top side of the hemisphere. Here, the maximum sound level reached is about $L_{p,max} = 23\,\mathrm{dB}$.

Table 2: Values for $L_{p,max}$ for Selected Frequencies.

f [Hz]	$L_{p,max}$ [dB]	f [Hz]	$L_{p,max}$ [dB]
100	-16	420	16
520	23	620	9
720	27	940	28
1040	11	1140	9

Table 2 collects the computed maximum sound-pressure levels for some selected frequencies. Although the highest force excitation is found for $f = 100\,\mathrm{Hz}$ (see Fig. 7) the resulting sound pressure on the hemisphere is the lowest. Its value is even below the auditory threshold. The highest levels are reached for the first stator- and rotor-slot harmonics at $f = 520\,\mathrm{Hz}$ and $f = 720\,\mathrm{Hz}$ as well as at $f = 940\,\mathrm{Hz}$. These

relations suit the structure-borne sound-measurements mentioned in the previous section by the proportion of the orders.

III.   CONCLUSION

In this paper the simulation of the electromagnetically excited structure- and air-borne noise of an induction machine with squirrel-cage rotor is described. The acoustic simulation is performed in three main steps and requires three different FEM/BEM models of the geometry of the machine. The structure-borne sound is derived from an intermediate step. The theory of the electromagnetic solvers is described as well as that of the structural-dynamic and the acoustic.

The main aspects which have to be regarded during the simulation are pointed out and some example pictures and tables show qualitative results. Detailed results will be presented in an additional paper concerning different types of surface-force excitation in the induction machine [13].

It is now possible to estimate the acoustic behavior of electrical devices. The structure-borne sound allows to simulate the deformation of the structure which is transmitted to other parts of the structure, e.g. the interior of a car.

IV.   REFERENCES

[1] Bastos, J. P. A., Sadowski, N., *Electromagnetic Modeling by Finite Element Methods*, Marcel Dekker, Inc., New York, Basel, 2003

[2] Zienkiewicz, O. C., Taylor, R. L., *The finite element method*, pages 346–361, McGraw-Hill Book Company, London, 1989

[3] Kost, A., *Numerische Methoden in der Berechnung elektromagnetischer Felder*, Springer-Verlag, Berlin, Heidelberg, New York, London, Paris, Tokyo, Hong Kong, Barcelona, Budapest, 1994

[4] Arians, G., Bauer, T., Kaehler, C., Mai, W., Monzel, C., van Riesen, D., Schlensok, C., "iMOOSE," www.imoose.de

[5] ANSYS Inc., www.ansys.com

[6] Ramesohl, I. H., Küppers, S., Hadrys, W., Henneberger, G., "Three Dimensional Calculation of Magnetic Forces and Displacements of a Claw-Pole Generator," *IEEE Transactions on Magnetics*, 32(3):1685–1688, May 1996

[7] Bronstein, I. N., Semendjajew, K. A., *Taschenbuch der Mathematik, 25. Auflage*, B. G. Teubner Verlagsgesellschaft, Stuttgart, Leipzig, 1991

[8] Schlensok, C., Schneeloch, G., Henneberger, G., "Analysis of Stator-Teeth Forces in Induction Machines with Squirrel Cages Using 2D-FEM," *6th International Symposium on Electric and Magnetic Fields*, EMF, Aachen, Germany, October 2003

[9] Nau, S. L., "Acoustic noise of induction electric motor: Causes and solutions," *2nd international Seminar on Vibrations and Acoustic Noise of Electric Machinery*, VANEM, Łódź, Poland, September 2000

[10] Jordan, H., *Geräuscharme Elektromotoren*, Verlag W. Girardet, Essen, 1950

[11] Ramesohl, I. H., *Numerische Geräuschberechnung von Drehstrom- Klauenpolgeneratoren*, Shaker Verlag, Aachen, 1999, Dissertation, Institut für Elektrische Maschinen, RWTH Aachen

[12] Seinsch, H. O., *Oberfelderscheinungen in Drehfeldmaschinen*, B. G. Teubner, Stuttgart, 1992

[13] Schlensok, C., Henneberger, G., "Comparison of Stator and Rotor Force Excitation for the Acoustic Simulation of an Induction Machine with Squirrel Cage Rotor," *16th International Conference on Electrical Machines*, ICEM, Crakow, Poland, September 2004